

# Synthesis of titanium-silver bimetallic nanoparticles by thermal plasma method

Sahar Shehni, Shahrooz Saviz\*, Amir Hosein Sari

## Abstract

In the present paper, the micron-size silver and titanium powder with desired weight ratios is used to produce the silver-titanium nanocomposite using the self-developed thermal plasma equipment. The mixture is fed into the plasma torch flame by the powder feed system and argon carrier gas. After evaporation, the particles are cooled inside the cooling chamber and collected from the surface of the water-cooled double-walled chamber. The production of Titanium-Silver bimetallic nanoparticles is achieved in two ways: the cooling chamber is once filled with argon and once with atmospheric air. The nanoparticles are analyzed using scanning electron microscope (SEM), Energy Dispersive X-ray Spectroscopy (EDS), and X-ray Diffraction (XRD) methods to identify the nanoparticle size distribution, morphology and chemical composition properties. The morphology of the produced nanocomposites is spherical and their average size is 30 nm. The results indicate that the average size of nanoparticles produced in the presence of air is smaller than those in the presence of argon.

## Keywords

Plasma spray, Thermal spraying, Silver nanoparticles, Titanium silver alloy, Coating layer.

*Plasma physics research center, Science and research branch, Islamic Azad University, Tehran, Iran.*

\*Corresponding author: shahrooz.saviz@srbiau.ac.ir

## 1. Introduction

Conventional production of nanoparticles faces two important issues: ability to produce in different scales, and high capability to achieve different chemical composition and morphology. Therefore, in addition to conventional methods, there is a need for a method that has higher potentials to meet these two conditions.

Monometallic nanoparticles are composed of a single metal. The properties of these nanoparticles are determined by their constituent atoms. Monometallic nanoparticles have different types characterized by the type of metal atoms, such as magnetic nanoparticles, metal and intermediate metals, and so on. Bimetallic nanoparticles [1, 2] are composed of two different metals and have, both scientifically and technologically, attracted greater attention than single metal nanoparticles [3, 4]. The constituent metals and their nanometer sizes determine the properties of bimetallic nanoparticles. Extensive studies in the field of bimetallic nanoparticles began only a decade ago. Various methods have since been proposed for the restoration and accurate description of these materials. Researchers these days are focusing on selectively producing new bimetallic nanoparticles in various forms such as alloys, core shells and contact aggregates. Researchers have discovered many new methods for developing nanoparticles which have the required size, composition and shape. In fact, these factors are the key to some of the most important properties of nanoparticles. Some of these methods include thermal and photochemical decomposition, electrochemical reduction, chemical reduction,

sputtering, Sol-gel method, chemical precipitation, Micro-emulsion and hydrothermal method.

Also recently, thermal plasma spray [5–9] has found important applications in the manufacturing of nanomaterials [10–17]. In plasma torches, electrons and ions reach an equilibrium temperature of about 10,000 °C. Therefore, they have a high density of energy. In addition, they contain various types of chemically active species including electrons and ions, radicals, and so on. There is also a very good temperature gradient in the flame of plasma torches. Such potential environments can produce reactions that are not thermodynamically desirable or require a lot of activating agents leading to the production of substances with abnormal chemical compounds or structures. Thermal plasma torches are now recognized as very effective, and in most cases unique, environments for converting materials into molten, evaporating and decomposing materials [12]. In this method, plasma torch is used together with some other accessories (Fig. 1) to produce nanoparticles. Control of the plasma torch parameters, control of physical and chemical conditions of the reaction chamber and control of nanoparticle cooling temperature are the main features of this method.

Lee et al. [13], Kuladeep et al. [14] and Grade et al. [15] synthesized Au-Ag alloy nanoparticles using pulsed laser ablation in water and a polyvinyl alcohol (PVA) solution, respectively. They examined the effect of laser pulse energy and time exposure on the particle size of the nanoparticles. The Ag-TiO<sub>2</sub> nanoparticles synthesized by sono-chemical and colloidal methods by Ramesh et al. [16] are spherical sub-

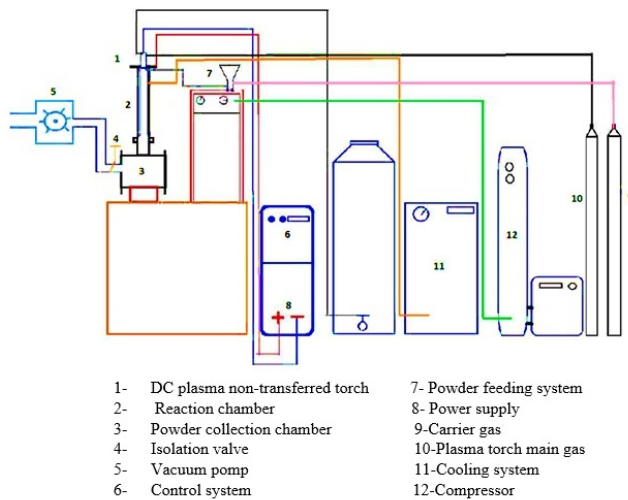


**Figure 1.** Schematic of the nanoparticle generation system.

stances with sizes in the range of 20 to 50 nm. Both Ag-TiO<sub>2</sub> and TiO<sub>2</sub> are generated via acid catalyzed sol-gel method innovated by S. aureus, P. aeruginosa and E. coli. Hamad and et al [17] generated the Ag-TiO<sub>2</sub> nanoparticles from Ag-Ti alloy raw materials with the aid of the laser ablation method. They also examined the antibacterial characteristics of the Ag-TiO<sub>2</sub> nanoparticles.

In this paper, the main goal is to produce titanium-silver bimetallic nanoparticles using the thermal plasma method. To this end, the generation of Ag-Ti bimetallic alloy by plasma spray method is demonstrated. Also, argon gas is inserted in the quench chamber and its effect on the physical and chemical characteristics of the Ag-Ti nanoparticles is investigated. The raw materials are micron-size silver and titanium particles that have been combined with a specific mass ratio.

## 2. Material and methods

### 2.1 Materials

Silver powder with a size of 60 micrometers and titanium powder with a size of 60 micrometers are used in this research.

### 2.2 Experimental tests

The tests used to analyze the synthesized samples in this study are SEM (FE-SEM, MIRA3 TESCAN-XMU), XRD (STOE Co. STADI MP), EDAX (TESCAN brand MIRA II model with SAMX detector made in France) and TEM (Philips EM208S 100KV) analysis.

### 2.3 Composite powder production method

In this study, Ti and Ag powders with a particle size of 60 micrometers are used to produce nano-composite powder with the aid of the thermal plasma spraying technique. For this purpose, the primary powders are first combined with specific combining ratios and mechanically milled through a rubbing mill for a certain time. Finally, the milled powder is rolled out uniformly using a method such as sifting.

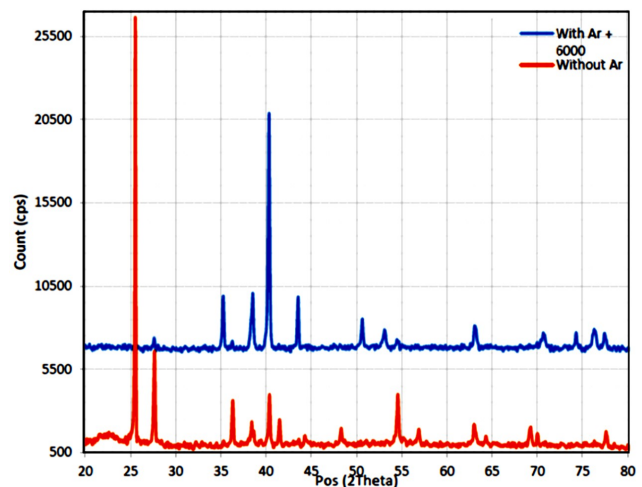


**Figure 2.** Comparison of the two spectra obtained from the sample with Argon and without Argon.

### 2.4 Plasma spraying and its parameters

In the next step, it is necessary to minify the milled powder to the Nano scale. For this purpose, we use the thermal plasma method which requires a plasma torch. The plasma torch used in this study is supported by a direct current (DC) source, and we have a tungsten cathode electrode that is in the form of a rod and a copper nozzle electrically insulated from each other. There is an air gap between the cathode and the anode, and the potential difference across them is 5 kV. In order to pass the current between anode and cathode, it is necessary to break this potential barrier. This is done by a high-voltage and high-frequency spark. When the spark is started in the air gap, the main power source transmits a high current between the cathode and the anode creating a high-temperature arc

**Table 1.** The results of network constant calculations for different elements.

Corresponding element	Peak angle (°)	Network constant (nm)
TiO <sub>2</sub>	27.6	0.644
Ti	35.5	0.505
Ag	38	0.472
Ti	38.5	0.467
Ti	40.35	0.446
Ag	43.57	0.415
Ti	53	0.345
TiO <sub>2</sub>	54.4	0.337
Ti	63	0.295
Ag	64	0.291
Ti	70.8	0.266
TiAg	76.3	0.249
TiAg	77.5	0.246

**Table 2.** Calculated crystalline size.

	Peak angle (°)	Maximum half width (°)	Average crystalline size (nm)
Without argon	56	0.18	51.79
	76.3	0.12	91.77
	77.5	0.28	38.09
With argon	64.4	0.06	170.59
	76.3	0.5	21.32
	77.5	0.27	39.19

between them. After creating a high-temperature arc, a gas such as argon, nitrogen etc. passes through the arc. In this study, argon is used as the main plasma torch gas. The gas passing through the arc is ionized and the plasma flame gets out of the nozzle. After the plasma flame is produced, the powder is inserted into the powder feeding device. These devices inject the powder into the plasma flame at a specific rate using powder vibration mechanism. The rate of powder injection into the plasma flame is very important as high flow rates can result in raw-burning state while low flow rates cannot produce nano particles. With the aid of the carrier gas, the particles inside the powder feeder are injected into the high-temperature plasma flame. The plasma torch current is about 500 A and the voltage is 50 V. When the powder enters the flame with this high temperature and velocity, it turns into a lava and goes down at a high speed and enters the reaction chamber. The reaction chamber is a two-wall enclosure which is filled with cool water with a temperature of 6-7 degrees circulating inside it. Therefore, the hot powder is hit by a cold wall, cracks away and breaks and slowly sticks to the enclosure wall. At this stage, the nano-powder is produced and can be collected. The atmosphere inside the reaction chamber can be evacuated and filled with a desired gas. In the present work, the reaction chamber is once filled with argon gas and then with air. When argon gas is used, the enclosure first gets vacuumed using a rotary pump. The pressure inside the enclosure is about 1 atm, and its material is stainless steel. A schematic representation of this process is shown in Fig. 1

### 2.5 Structural characterization of powder and coating particles - XRD and SEM

For the XRD analysis, the starting and final angles are 10 degrees and 100 degrees, respectively with a measurement step of 0.03 degrees. The measurement time is 720 seconds. The anode material is copper. The voltage used for the SEM device is 25 kV and the magnification is 80,000 times. Also, the sample scan time is 111 seconds.

**Table 3.** Comparison of the area under the XRD peaks (Arb. unit).

Peak location (°)	Element	Without argon	With argon
25.5	TiO <sub>2</sub> Anatase	24837.19	-
27.6	TiO <sub>2</sub> Rutile	62933.03	15104.76
35.5	Ti	-	41334
36.3	TiO <sub>2</sub> Rutile	45134.42	-
38	Ag	12986.19	20179
38.5	Ti	22306.47	52937
38.3	TiO <sub>2</sub> Anatase	12985.81	-
39.2	TiO <sub>2</sub> Rutile	16843.05	-
40.35	Ti	55027.93	142666
41.3	TiO <sub>2</sub> Rutile	29055.51	-
43.57	Ag	-	34439.77
44.3	Ag	26697.05	-
48	TiO <sub>2</sub> Anatase	33206.7	-
53	Ti	-	37514
54	TiO <sub>2</sub> Anatase	19538	-
54.4	TiO <sub>2</sub> Rutile	46020	22938
55.2	TiO <sub>2</sub> Anatase	24453	-
56	TiAg	15624	-
57	TiO <sub>2</sub> Rutile	30622	-
63	TiO <sub>2</sub> Anatase	36552	-
63	Ti	-	41069
64	Ag	14019	7741
64.4	TiAg	18526	7747
69.2	TiO <sub>2</sub> Rutile	35168	-
70	TiO <sub>2</sub> Rutile	18876	-
70.8	Ti	-	42739.93
74.3	Ti	-	27979.1
76.3	TiAg	8426.65	40627.98
77.5	TiAg	18727.61	30196.6
77.5	Ag	20246.49	-

### 2.6 Combined characterization of sample (EDAX)

The voltage used for the EDAX device is 25 kV and the test time is 28.7 seconds. The resolution of this device is 129.7 eV.

## 3. Results and discussion

### 3.1 XRD Analysis

X-ray results for samples produced in the presence of argon and its absence are shown in Fig. 2. For quantitative analysis, first the peaks are determined and the intensity and angle of each peak are extracted from the obtained spectra. According to the specification and based on Bragg law, it is found that the smaller the peak angle, the more spacing the pages have. The results of the network constant calculation for each element are shown in Table 1.

In order to calculate the average size of crystals, the Debye-

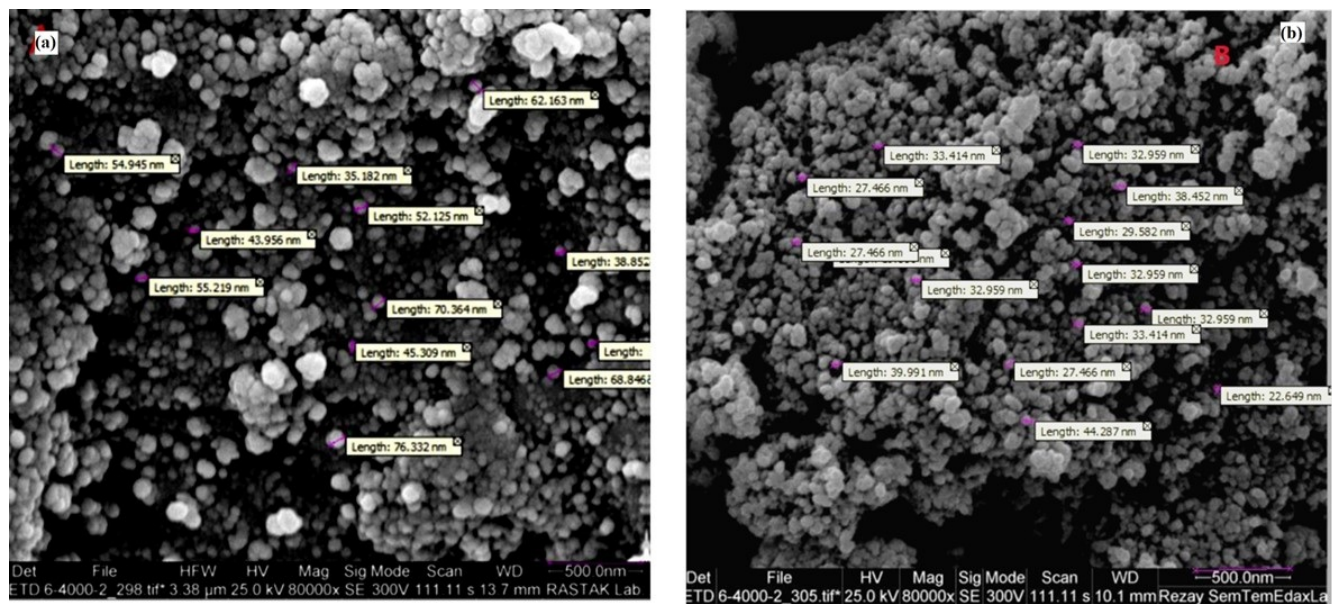


**Figure 3.** Comparison of the dimensions of the formed nanoparticles and the amount of oxide in the two samples a) with argon, and b) without argon.

Scherer formula is used [4]:

$$D = 0.94 \frac{\lambda}{\beta \cos \theta} \tag{1}$$

where  $D$  is the mean particle size,  $\theta$  is the Bragg's diffraction angle,  $\lambda$  is the wavelength of the X-rays and  $\beta$  is the half-width of the maximum intensity. For this purpose, we first consider the TiAg peaks at  $2\theta$  and obtain the peak width at half intensity. It should be noted that this value should be in radians. Given the Debby-Scherer correlation, it can be seen that FWHM increases for smaller particle size of the material. This means that the peak gets wider and less intense. In other words, the peak of nanoparticles is less intense and wider than those of conventional materials. The results of size calculation for crystals are shown in Table 2.

Figure 2 shows the XRD analysis of the Ag-Ti nanocompos-

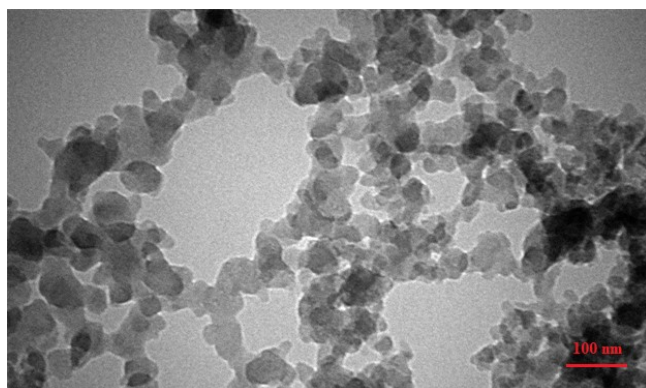


**Figure 4.** TEM-image of Ti-Ag bimetallic nanoparticles.

ite both in the presence and absence of argon. The difference

between the two spectra is in the intensity of the peaks and the presence of different elements in each sample. We now examine the location of the peaks and their intensity for the two samples (Table 3). As shown in Table 3, the total area under the curves related to  $TiO_2$  for a sample without argon is 218111 and that of the sample with argon is 38042. In other words, the rate of oxidation in the absence of argon is about 5.7 times that in the presence of argon.

The total area under the curves related to TiAg nanocomposite for a sample without argon is 61303 and that of the argon-containing sample is 78570. In other words, the production of silver-titanium nanocomposites in the presence of argon is 1.28 times higher than when it is absent. Finally, the following results are obtained from the XRD analysis:

1. In the presence of the noble argon gas in the quench chamber, oxygen concentration in the environment is much lower. Therefore, there are fewer and less intense characteristic peaks of  $TiO_2$  in the sample spectra in the presence of argon while these peaks are found abundantly and with high intensity in the spectra of argon-free samples.
2. In the sample without argon, a relatively high percentage of titanium is converted into titanium oxide and the concentration of TiAg in this sample is less than that in the sample with argon.
3. Two different structures of the  $TiO_2$  composition are visible in the sample without argon: Anatase and Rutile. The difference between the two is in their dimensions which has previously been studied in the analysis of the elements in the spectrum. Since the production of nanoparticles has been accompanied by heat treatment, various temperature regimes of the production process of nanoparticles can be cited as the cause of forming these structures.

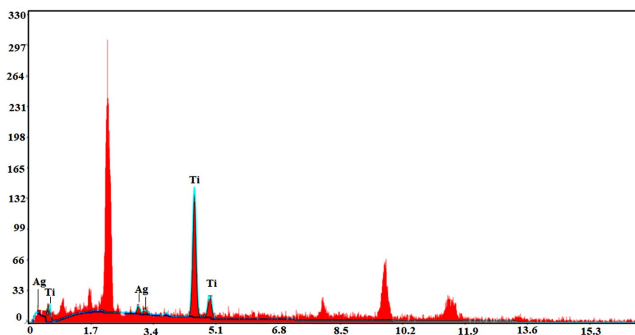


Figure 5. EDAX results for example in the presence of argon.

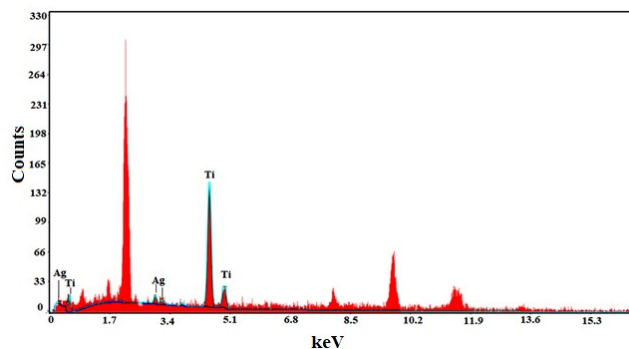


Figure 6. EDAX results for the sample without argon.

### 3.2 Analysis of the results obtained from SEM

In this section, images taken by a scanning electron microscope are presented as Figs. 3-6. As can be seen, in the presence of argon, the size of the formed nanoparticles is from at least 35.182 nm to a maximum of 76.332 nm which is in the typical range of nanoparticles material. The size of the nanoparticles in the argon-free sample ranges from 22,649 nm to 44,287 nm. The reason for the differences in the dimensions of these two samples is the effect of argon on the temperature of the production process. As shown in the results of the crystal structure analysis, temperature affects the formation of compound structures.

Another noticeable observation is the higher oxide content in argon-free samples (B) which is well seen on all scales. The oxide material is seen in black in images taken by SEM and the darker areas in the image correspond to the higher oxygen content in the sample environment and, therefore, the greater oxide compounds.

In general, Ag, Ti and TiAg compounds are well-formed in both samples. The dimensions of the nanoparticle are within the acceptable range and the nanoparticles are well distributed in the material media (according to the SEM results) and across the thickness of the material (according to the XRD results). As seen in Fig. 3, the nano particles are in a spherical form.

### 3.3 TEM Analysis

Figures 4 present characteristic TEM images of bimetallic Ti–Ag nanoparticles. As seen in this figure the particles are spherical.

### 3.4 Analysis of the EDAX

Figure 5 shows the EDAX analysis in the presence of argon. The silver content of the sample in the presence of argon is 3.54 wt% and that of titanium is 96.44wt%.

Figure 6 shows the EDAX analysis in the absence of argon. The silver content of the sample in the absence of argon is 6.84 wt% and that of titanium is 93.16 wt%. As can be seen, the results of EDAX are consistent with the results of the sample's crystal structure analysis. The higher concentration of silver in the argon-free sample is attributed to its high

oxide concentration. As the TiO<sub>2</sub> concentration increases, the chance of forming Ti–Ag link is lowered, so higher silver content is observed in this sample.

## 4. Conclusion

Thanks to the rapid scientific advances and the application of new technologies in the industry, plasma physics has become one of the branches of physics widely used in the modern industry. Given the extensive applications of plasma torch in the industry, this study examines the nanostructures of bimetallic powder produced by this method. The plasma torch is used for coating and is also known as the plasma spray.

Plasma Spray is a method for providing abrasion-resistant coating in which metal powder and high melting point powders are sprayed onto the substrate. Recently, the use of plasma sprays have diversified. Hot plasma has high temperature, high enthalpy and high thermal gradient. In the plasma-spraying process, the coating material enters the plasma torch flame. In this process, the raw materials are initially in powder form and are turned into molten or semi-molten particles through thermal or explosive methods. Once sprayed, these particles stick on the surface thus forming layers on each other. This coating method is used to enhance and increase the resistance to corrosion, erosion, and thermal insulation.

This research attempted to produce titanium/silver bimetallic nano powder composite using plasma spray method. Evaluation of the results of SEM obtained from fabricated samples confirm the formation of nanoscale structures. The SEM results also indicate that in the sample containing argon, the size of the nanoparticles ranges from 35.182 nm to 76.332 nm which is typical of common nanoparticles. The size of these nanoparticles in an argon-free sample varies from 22.649 nm to a maximum of 44.287 nm. The reason for the differences in the dimensions of these two samples is the effect of argon on the temperature of the production process. As observed in the of results of the crystal structure analysis, the temperature influences the formation of compound structures.

Another important point in this study is the higher amount of oxide material in non-argon samples which is well seen on all scales. The oxide material in the photos obtained from the SEM is seen in dark areas with the darker areas corresponding

to the higher oxygen content in the sample media and, therefore, the higher concentrations of oxide compounds.

Also, as observed in the x-ray diffraction patterns of the samples, the total number of peaks associated with TiO<sub>2</sub> for the sample without argon is 218111 whereas for the sample with argon it is 38042. In other words, the proportion of the oxidation process in the sample with the presence of argon is only about 17% of that in the absence of argon.

The total number of peaks of Ti-Ag-related peaks for an argon-free sample is 61303 and that of a sample with argon is 78570. In other words, the ratio of peak instances in the specimen with the presence of argon is 120% of that in its absence meaning that the Ti-Ag compound in plasma spray in the presence of argon is 20% more than in the presence of oxygen.

By comparing the curves of X-ray diffraction spectra in different samples with index spectra, it can be concluded that:

- Since the oxygen concentration in the environment is much lower in the presence of noble argon gas, the characteristic peaks of TiO<sub>2</sub> in the sample spectra in the presence of argon are very few and with little intensity. However, these peaks are found abundantly in the spectra of argon-free samples.

- In the argon-free sample, a relatively high percentage of titanium is converted into titanium oxide. Therefore, the concentration of Ti-Ag in this sample is less than that in the argon-containing sample. Consequently, the concentration of Ag not added to the compound is higher in the sample without argon than the argon-containing sample.

- Two different structures of TiO<sub>2</sub> compounds are visible in the argon-free sample: Anatase and Rutile. The difference between the two is in their dimensions which has previously been studied in the analysis of the elements in the spectrum. Since the production of nanoparticles has been accompanied by heat treatment, various temperature regimes for nanoparticle production process can be mentioned as the cause of these structures.

#### Conflict of interest statement:

The authors declare that they have no conflict of interest.

## References

- [1] G. Sharma, A. Kumar, S. Sharma, M. Naushad, R.P. Dwivedi, Z.A. AlOthman, and G.T. Mola. *Journal of King Saud University-Science*, **31**:257, 2019.
- [2] S.H. Chang, M.H. Yeh, J. Rick, W.N. Su, D.G. Liu, J.F. Lee, C.C. Liu, and B.J. Hwang. *Sensors and Actuators B: Chemical*, **190**:55, 2014.
- [3] G. Sharma, M. Naushad, H. Aláa, A. Kumar, M.R. Khan, S. Kalia, M. Bala, and A. Sharma. *International journal of biological macromolecules*, **95**:484, 2017.
- [4] N. Toshima and T. Yonezawa. *New Journal of Chemistry*, **22**:1179, 1998.
- [5] P.R. Taylor and 1(1) (1994) 35-50. S. A. Pirzada. *Advanced Performance Materials*, **1**:35, 1994.
- [6] S. Saviz F. Rezaei and 12(1) (2018) 1-6. M. Ghoranneviss. *Journal of Theoretical and Applied Physics*, **12**:1, 2018.
- [7] S. Khandanjou, M. Ghoranneviss, S. Saviz, and M.R. Afshar. *Chinese Physics B*, **27**:028104, 2018.
- [8] G. Masoumeh, S. Saviz, G. Ghoranneviss, and S. E. Ahmad. *Journal of Theoretical and Applied Physics*, **12**:85, 2018.
- [9] M. I. Boulos, P. Fauchais, and E. Pfender. *Thermal Plasmas: Fundamentals and Applications*, **1**:58, 1994.
- [10] J.H. Seo and B.G. Hong. *Nuclear engineering and technology*, **44**:9, 2012.
- [11] C.M. Crisan, T. Mocan, M. Manolea, L. I. Lasca, F. A. Tãbãřan, and L. Mocan. *Applied Sciences*, **11**:1120, 2021.
- [12] K.S. Kim and T. H. Kim. *Journal of Applied Physics*, **125**:070901, 2019.
- [13] I. Lee, S. W. Han, and K. Kim. *Chemical Communications*, **18**:1782, 2001.
- [14] R. Kuladeep, L. Jyothi, K. S. Alee, K.L.N. Deepak, and D.N. Rao. *Optical Materials Express*, **2**:161, 2012.
- [15] S. Grade, J. Eberhard, J. Jakobi, A. Winkel, M. Stiesch, and S. Barcikowski. *Gold Bulletin*, **47**:83, 2014.
- [16] P. Ramesh, S. Muthukumarasamy, K. Dhanabalan, T. Sadhasivam, and K. Gurunathan. *Dig J Nanomater Biostruct*, **7**:1501, 2012.
- [17] A. Hamad, L. Li, Z. Liu, X.L. Zhong, H. Liu, and T. Wang. *Rsc Advances*, **5**:7981, 2015.